OPT-*i*
An International Conference on
Engineering and Applied Sciences Optimization
M. Papadrakakis, M.G. Karlaftis, N.D. Lagaros (eds.)
Kos Island, Greece, 4-6, June 2014

ADJOINT METHODS FOR SHAPE OPTIMIZATION AND ROBUST DESIGN IN FLUID MECHANICS

Kyriakos C. Giannakoglou, Dimitrios I. Papadimitriou, Evangelos M. Papoutsis-Kiachagias and Ioannis S. Kavvadias

National Technical University of Athens,
School of Mechanical Engineering,
Lab. Of Thermal Turbomachines,
Parallel CFD & Optimization Unit
Zografou, Athens, 15710, Greece
e-mails: kgianna@central.ntua.gr, dpapadim@mail.ntua.gr, vaggelisp@gmail.com,
kavvadiasj@hotmail.com

Keywords: Continuous Adjoint Approach, Shape Optimization, High-Order Derivatives, Robust Design

Abstract. *This paper presents adjoint methods for the computation and use of the first- and higher-order sensitivity derivatives of objective functions F in optimization problems governed by PDEs, in aero/hydrodynamics. In the first part, the continuous adjoint approach to widely-used turbulence models, such as the Spalart-Allmaras and k-ε one is presented in their low-Reynolds and high-Reynolds (with wall functions) variants. The relevant developments allow the computation of the exact gradient of the objective function using continuous adjoint, even for RANS assisted by wall functions, and overcome the frequently made assumption of negligible turbulence variations. The second part of this paper deals with higher-order sensitivity analysis based on the combined use of the adjoint approach and direct differentiation. For robust design problems, the computation of second-order derivatives w.r.t. the environmental variables aiming at the computation of the first two statistical moments is required; if in addition, the problem is to be solved using a descent algorithm, third-order mixed derivatives w.r.t. both environmental and design variables must be available; optimal ways to perform these computations are demonstrated. This paper goes through both continuous and (hand-differentiated) discrete adjoint methods. In the last part, some other relevant recent achievements regarding the adjoint approach are discussed. Regarding applications, the adjoint method is demonstrated for various objective functions and used to solve aero/hydrodynamic shape optimization problems, optimization of jet-based flow-control systems for controlling the development of boundary layers and topology optimization problems in fluid mechanics. Depending on the problem, the development relies upon the incompressible or compressible fluid flow equations.*

1 FLOW EQUATIONS AND OBJECTIVE fUNCTIONS

Before presenting the formulation of the continuous adjoint method [] for turbulent flows, the equations governing the state (i.e. flow) problem are briefly presented. This presentation is made for an incompressible fluid flow using either the one-equation Spalart-Allmaras [1] or the Jones-Launder $k-\varepsilon$ [2] turbulence models. The mean flow state equations are

$$R^p = \frac{\partial v_j}{\partial x_j} = 0 \tag{1}$$

$$R^{v_i} = v_j \frac{\partial v_i}{\partial x_j} + \frac{\partial p}{\partial x_i} - \frac{\partial}{\partial x_j}\left[(\nu+\nu_t)\left(\frac{\partial v_i}{\partial x_j}+\frac{\partial v_j}{\partial x_i}\right)\right] = 0 \tag{2}$$

v_i are the velocity components, p is the static pressure divided by the density, T is the static temperature, ν is the bulk viscosity and Pr, Pr_t are the laminar and turbulent Prandtl numbers. ν_t is the turbulent viscosity computed by solving the turbulence model equation(s),

$$R^{\widetilde{\nu}} = v_j \frac{\partial \widetilde{\nu}}{\partial x_j} - \frac{\partial}{\partial x_j}\left[\left(\nu+\frac{\widetilde{\nu}}{\sigma}\right)\frac{\partial \widetilde{\nu}}{\partial x_j}\right] - \frac{c_{b_2}}{\sigma}\left(\frac{\partial \widetilde{\nu}}{\partial x_j}\right)^2 - \widetilde{\nu}P\left(\widetilde{\nu}\right) + \widetilde{\nu}D\left(\widetilde{\nu}\right) \tag{3}$$

in the case of the Spalart-Allmaras model and

$$\begin{aligned} R^k &= v_j \frac{\partial k}{\partial x_j} - \frac{\partial}{\partial x_j}\left[\left(\nu+\frac{\nu_t}{Pr_k}\right)\frac{\partial k}{\partial x_j}\right] - P_k + \epsilon + D = 0 \\ R^\epsilon &= v_j \frac{\partial \epsilon}{\partial x_j} - \frac{\partial}{\partial x_j}\left[\left(\nu+\frac{\nu_t}{Pr_\epsilon}\right)\frac{\partial \epsilon}{\partial x_j}\right] - c_1 P_k \frac{\epsilon}{k} + c_2 f_2 \frac{\epsilon^2}{k} - E = 0 \end{aligned} \tag{4}$$

in the case of the k-ε model. $\widetilde{\nu}$ is the turbulence state variable, in the Spalart-Allmaras model and k, ϵ are the corresponding quantities (turbulent kinetic energy and turbulent energy dissipation) in the k-ϵ model. In both cases the boundary conditions and the model constant values are omitted in the interest of space; their values may be found in [1] and [2]. For the closure, $\nu_t = \widetilde{\nu} f_{v_1}$ in the Spalart-Allmaras model and $\nu_t = c_\mu \frac{k^2}{\varepsilon}$ in the k-ϵ one.

The objective function, written in general form comprises both surface and volume integrals, as follows

$$F = \int_S F_S dS + \int_\Omega F_\Omega d\Omega = \int_S F_{S_i} n_i dS + \int_\Omega F_\Omega d\Omega \tag{5}$$

where F_S and F_Ω are the integrands on the boundary and volume of the domain, respectively, where n_i is the outward unit normal vector

2 THE ADJOINT METHOD FOR SHAPE OPTIMIZATION IN TURBULENT FLOWS

Even though in discrete adjoint the differentiation of the turbulence model equations is straightforward and can be found in several published works, [3, 4], in continuous adjoint the majority of the existing works rely on the so-called "frozen turbulence" assumption, in which the sensitivities of the turbulence quantities w.r.t. the design variables are neglected [5, 6, 7, 8, 9]. The first work presenting the adjoint to one of the most widely used turbulence models, namely the Spalart-Allmaras one, for incompressible flows, is [10]. Later on, this was extended to compressible flows in [11]. Regarding the adjoint approach to high-Reynolds turbulence models, the (continuous) adjoint to the k-ε model with wall functions has been recently presented in the literature, [12], whereas the continuous adjoint to the low-Reynolds Launder-Sharma k-ε model has been presented in [13].

2.1 The Adjoint Approach to Low-Reynolds Turbulence Models

In the continuous adjoint approach for shape optimization problems, the total sensitivity derivatives (symbol δ) of any function Φ w.r.t. b_m are related to the corresponding partial sensitivities (symbol ∂) through the relation

$$\frac{\delta\Phi}{\delta b_m} = \frac{\partial\Phi}{\partial b_m} + \frac{\partial\Phi}{\partial x_l}\frac{\delta x_l}{\delta b_m} \tag{6}$$

where $\frac{\delta x_l}{\delta b_i}$ are the sensitivities of nodal coordinates.

For an arbitrary quantity Φ computed on a surface, the above equation takes the specific form $\frac{\delta_s\Phi}{\delta b_n} = \frac{\partial\Phi}{\partial b_n} + \frac{\partial\Phi}{\partial x_k}n_k\frac{\delta x_m}{\delta b_n}n_m$ Since any sufficiently small surface deformation can be seen as a normal perturbation, only the normal part of the surface deformation velocity $\delta x_k/\delta b_n$ causes a change in Φ

In order to formulate the adjoint equations, the augmented objective function F_{aug} is defined as the sum of F and the field integrals of the products of the adjoint variable fields and the state equations, as follows

$$F_{aug} = F + \int_\Omega u_i R_i^v d\Omega + \int_\Omega q R^p d\Omega + E_{TM} \tag{7}$$

where u_i are the adjoint velocity components, q is the adjoint pressure, and the extra terms E_{TM} depend on the turbulence model (TM). In Spalart-Allmaras ($TM = SA$)

$$E_{SA} = \int_\Omega \widetilde{\nu_a} R^{\tilde{\nu}} d\Omega \tag{8}$$

whereas in the k-ϵ model ($TM = KE$)

$$E_{KE} = \int_\Omega \left(k_a R^k + \epsilon_a R^\epsilon\right) d\Omega \tag{9}$$

where $\widetilde{\nu_a}$, k_a and ϵ_a are the adjoints to $\widetilde{\nu}$, k and ϵ, respectively.

Based on the Leibniz theorem, the derivative of the augmented objective function w.r.t. b_n reads

$$\frac{\delta F_{aug}}{\delta b_n} = \frac{\delta F}{\delta b_n} + \int_\Omega u_i\frac{\partial R_i^v}{\partial b_n}d\Omega + \int_\Omega q\frac{\partial R^p}{\partial b_n}d\Omega + \int_{S_{W_p}}\left(u_i R_i^v + qR^p\right)\frac{\delta x_k}{\delta b_n}n_k dS + \frac{\delta(E_{TM})}{\delta b_m} \tag{10}$$

where

$$\frac{\delta(E_{SA})}{\delta b_m} = \int_\Omega \widetilde{\nu_a}\frac{\partial R^{\tilde{\nu}}}{\partial b_n}d\Omega + \int_{S_{W_p}}\widetilde{\nu_a}R^{\tilde{\nu}}\frac{\delta x_k}{\delta b_n}n_k dS \tag{11a}$$

$$\frac{\delta(E_{KE})}{\delta b_m} = \int_\Omega k_a\frac{\partial R^k}{\partial b_n}d\Omega + \int_\Omega \epsilon_a\frac{\partial R^{\epsilon_a}}{\partial b_n}d\Omega + \int_{S_{W_p}}\left(k_a R^k + \epsilon_a R^\epsilon\right)\frac{\delta x_k}{\delta b_n}n_k dS \tag{11b}$$

After a lengthy development of the volume integrals in eq. 10, based on the Green-Gauss theorem, and the elimination of the terms that depend on the sensitivities of the mean flow and turbulence model variables, the adjoint to the mean flow equations yield

$$R^q = -\frac{\partial u_j}{\partial x_j} = 0 \tag{12}$$

$$R_i^u = u_j\frac{\partial v_j}{\partial x_i} - \frac{\partial(v_j u_i)}{\partial x_j} - \frac{\partial}{\partial x_j}\left[(\nu+\nu_t)\left(\frac{\partial u_i}{\partial x_j}+\frac{\partial u_j}{\partial x_i}\right)\right] + \frac{\partial q}{\partial x_i} + AMS_i = 0\ ,\ i = 1,2(,3) \tag{13}$$

The extra terms in the adjoint momentum equations (AMS_i), arising from the differentiation of the turbulence model, can be found in [10, 13]. The adjoint turbulence model variables' fields $\widetilde{\nu_a}, k_a$ and ϵ_a are governed by the adjoint turbulence model PDEs, which are as follows

$$\begin{aligned}
R^{\widetilde{\nu_a}} =& -\frac{\partial(v_j\widetilde{\nu_a})}{\partial x_j} - \frac{\partial}{\partial x_j}\left[\left(\nu+\frac{\widetilde{\nu}}{\sigma}\right)\frac{\partial\widetilde{\nu_a}}{\partial x_j}\right]+\frac{1}{\sigma}\frac{\partial\widetilde{\nu_a}}{\partial x_j}\frac{\partial\widetilde{\nu}}{\partial x_j}+2\frac{c_{b2}}{\sigma}\frac{\partial}{\partial x_j}\left(\widetilde{\nu_a}\frac{\partial\widetilde{\nu}}{\partial x_j}\right)+\widetilde{\nu_a}\widetilde{\nu}\mathcal{C}_{\widetilde{\nu}}\\
&+\frac{\partial\nu_t}{\partial\widetilde{\nu}}\frac{\partial u_i}{\partial x_j}\left(\frac{\partial v_i}{\partial x_j}+\frac{\partial v_j}{\partial x_i}\right)+(-P+D)\,\widetilde{\nu_a}=0 \qquad (14a)\\
R^{k_a} =& -\frac{\partial(v_jk_a)}{\partial x_j}-\frac{\partial}{\partial x_j}\left[\left(\nu+\frac{\nu_t}{Pr_k}\right)\frac{\partial k_a}{\partial x_j}\right]\\
&+\left(\frac{B_1}{Pr_k}-\frac{\nu}{k}\right)\frac{\partial k}{\partial x_j}\frac{\partial k_a}{\partial x_j}+\frac{B_1}{Pr_\epsilon}\frac{\partial\epsilon}{\partial x_j}\frac{\partial\epsilon_a}{\partial x_j}+B_1\left(\frac{\partial v_i}{\partial x_j}+\frac{\partial v_j}{\partial x_i}\right)\frac{\partial u_i}{\partial x_j}\\
&+\left[\frac{\nu}{2k^2}\left(\frac{\partial k}{\partial x_j}\right)^2-\frac{\nu}{k}\frac{\partial^2k}{\partial x_j^2}-PB_1\right]k_a\\
&-\left[c_1\frac{\epsilon}{k}PB_1+2\nu\left(\frac{\partial^2v_k}{\partial x_i\partial x_j}\right)^2B_1+c_2f_2\frac{\epsilon^2}{k^2}-1.2c_2\frac{k^2}{\nu^2}e^{-Re_t^2}-c_1P_k\frac{\epsilon}{k^2}\right]\epsilon_a=0 \qquad (14b)\\
R^{\epsilon_a} =& -\frac{\partial(v_j\epsilon_a)}{\partial x_j}-\frac{\partial}{\partial x_j}\left[\left(\nu+\frac{\nu_t}{Pr_\epsilon}\right)\frac{\partial\epsilon_a}{\partial x_j}\right]\\
&+\frac{B_2}{Pr_\epsilon}\frac{\partial\epsilon}{\partial x_j}\frac{\partial\epsilon_a}{\partial x_j}+\frac{B_2}{Pr_k}\frac{\partial k}{\partial x_j}\frac{\partial k_a}{\partial x_j}+B_2\left(\frac{\partial v_i}{\partial x_j}+\frac{\partial v_j}{\partial x_i}\right)\frac{\partial u_i}{\partial x_j}+(1-PB_2)\,k_a\\
&+\left[-2\nu\left(\frac{\partial^2v_k}{\partial x_i\partial x_j}\right)^2B_2-c_1\frac{\epsilon}{k}PB_2+2c_2f_2\frac{\epsilon}{k}-0.6c_2\frac{k^3}{\nu^2\epsilon}e^{-Re_t^2}-c_1P_k\frac{1}{k}\right]\epsilon_a=0 \qquad (14c)
\end{aligned}$$

The detailed derivation of the adjoint equations and the corresponding adjoint boundary conditions can be found in [10] or [13].

After satisfying the field adjoint equations, the sensitivity derivatives of the objective function takes the following form

$$\begin{aligned}
\frac{\delta F_{aug}}{\delta b_n} =& \int_S\mathcal{BC}_i^u\frac{\partial v_i}{\partial b_n}dS+\int_S(u_jn_j+\frac{\partial F_{S_i}}{\partial p}n_i)\frac{\partial p}{\partial b_n}dS+\int_S(-u_in_j+\frac{\partial F_{S_k}}{\partial\tau_{ij}}n_k)\frac{\partial\tau_{ij}}{\partial b_n}dS\\
&+\int_{S_{W_p}}n_i\frac{\partial F_{S_{W_p,i}}}{\partial x_m}n_m\frac{\delta x_k}{\delta b_n}n_kdS+\int_{S_{W_p}}F_{S_{W_p,i}}\frac{\delta n_i}{\delta b_n}dS+\int_{S_{W_p}}F_{S_{W_p,i}}n_i\frac{\delta(dS)}{\delta b_n}\\
&+\int_{S_{W_p}}(u_iR_i^v+qR^p)\frac{\delta x_k}{\delta b_n}n_kdS+\mathcal{SD} \qquad (15)
\end{aligned}$$

where, depending on the turbulence model, the missing terms $\mathcal{BC}_i$ and $\mathcal{SD}$ may be found in [10] or [13]. The gain from overcoming the "frozen turbulence" assumption is shown in selected cases. It is demonstrated that, the "frozen turbulence" assumption may lead to sensitivities which might even have the wrong sign, misleading thus the descent process. Such an example, concerning the flow in a 90^o elbow duct, with a Reynolds number equal to 3.5×10^4, modeled using the Spalart–Allmaras model is given in fig. 1 [10].

The shape optimization of an S-shaped duct targeting minimum total pressure losses $F=-\int_{S_I}\left(p+\frac{1}{2}v^2\right)v_in_idS-\int_{S_O}\left(p+\frac{1}{2}v^2\right)v_in_idS$ is investigated in fig. 2. The flow Reynolds number based on the inlet height is $Re=1.2\times10^5$ and the Launder–Sharma $k-\epsilon$ model is used. The

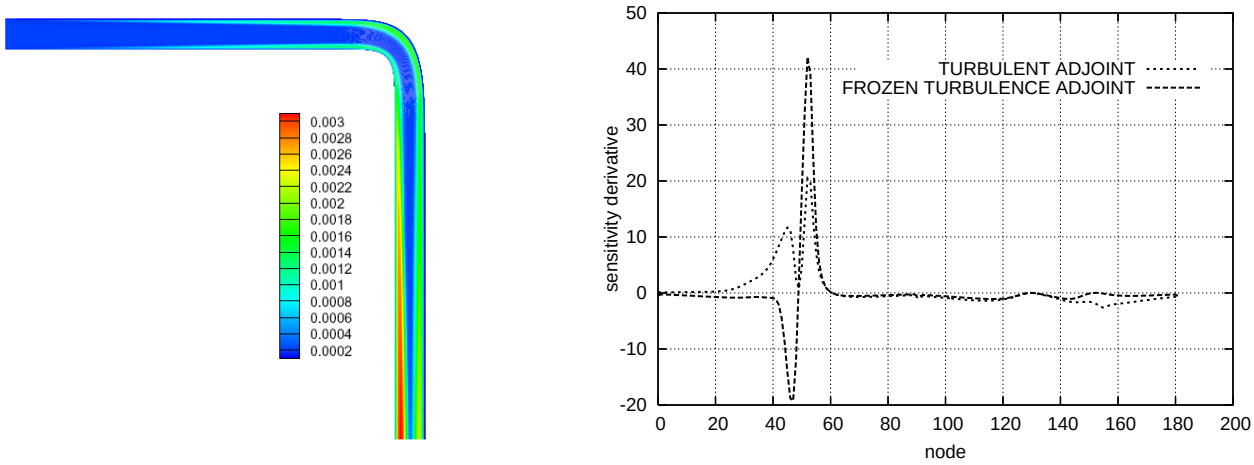

Figure 1: Adjoint to the low-Re Spalart–Allmaras model: Left: pressure field plotted on a 90^o elbow duct with constant cross section; Right: sensitivity derivatives of the total pressure losses function $\delta F/\delta b_n$, where b_n are the normal displacements of the solid wall grid nodes. Two sensitivity distributions are compared (a) the outcome of the complete adjoint approach (marked as "turbulent adjoint") and (b) the outcome of an adjoint solver making the "frozen turbulence" assumption (marked as "frozen turbulence adjoint"). The abscissa stands for the nodal numbers of the wall nodes. By making the "frozen turbulence" assumption, wrongly signed sensitivities are computed between nodes 20 and 50. Extensive validation of the adjoint solver against direct differentiation in conducted in [10].

upper and lower duct contours are parameterized using Bézier–Bernstein polynomials with 12 control points each. Two gradient–based optimization methods, namely steepest descent and the Fletcher-Reeves Conjugate Gradient (CG) method are used. The gradients used by each method to update the design variables are based on (a) the proposed method to compute $\delta F/\delta b_n$ and (b) adjoint with the "frozen turbulence" assumption. The starting duct shape along with the optimal ones computed by the steepest descent method, based on the two variants of the adjoint formulation, are presented in fig. 2-top. Both have reached the same result. The shape resulting from variant (a) has an objective function value that is about 3% lower than that of variant (b) and reaches the optimal solution after approximately 30% less cycles than that using the "frozen turbulence" assumption. The beneficial impact of differentiating the turbulence model on the optimization procedure is reconfirmed for the CG method, fig. 2-bottom, where with the exact sensitivity derivatives, a 20% economy in the number of optimization cycles is observed.

2.2 The Adjoint Approach to High-Reynolds Turbulence Models

In industrial projects, many analysis codes rely on the use of the wall function techniques, due to the less stretched meshes and the economy in the overall CPU cost. The development of the adjoint approach to the wall function model is thus necessary.

Regarding the k-ϵ model, this development was based on a vertex-centered finite volume code with non-zero slip velocity at the wall. The real solid wall is assumed to lie at a distance Δ underneath the grid boundary marked as solid "wall". Integrating the state equations over the vertex-centered finite volume of fig. 3, the diffusive flux through the segment $\alpha\beta$ depends on the friction velocity v_τ,

$$v_\tau^2 = (\nu + \nu_t)\left(\frac{\partial v_i}{\partial x_j} + \frac{\partial v_j}{\partial x_i}\right) n_j t_i \tag{16}$$

where v_τ is computed via the law of the wall. Based on the latter, if P belongs to either the log

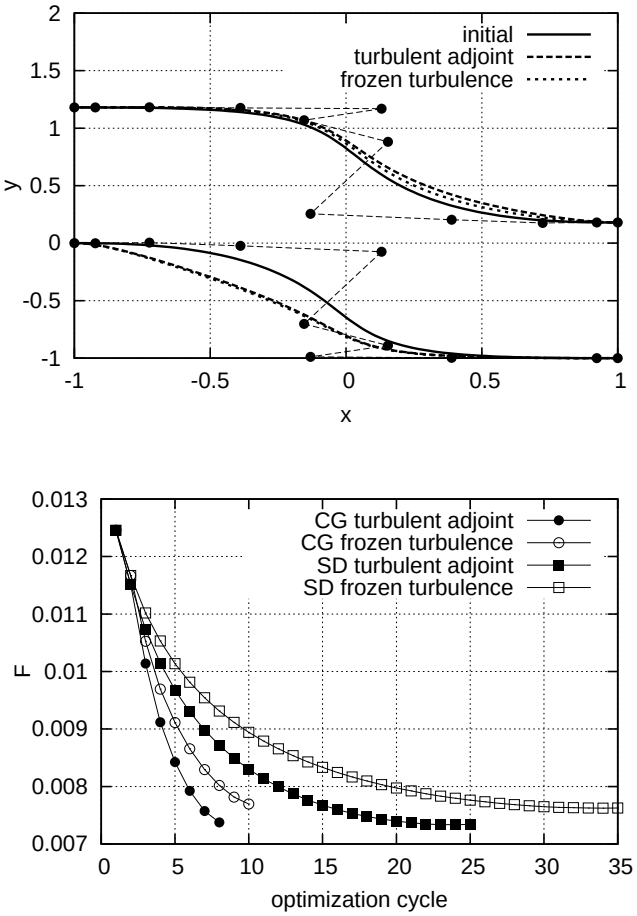

Figure 2: Adjoint to the low-Reynolds Launder–Sharma $k-\epsilon$ model: Shape optimization of an S-shaped duct targeting minimum total pressure losses. Top: starting duct shape compared to the optimal solutions resulting from the steepest descent algorithm that uses (a) the proposed method to compute $\delta F/\delta b_n$ ("turbulent adjoint") and (b) the adjoint method based on the "frozen turbulence" assumption ("frozen turbulence"); axes are not in scale. Bottom: Convergence history of two optimization algorithms (steepest descent, SD, and conjugate gradient, CG) driven by different adjoint methods. From [13].

law region or the viscous sublayer, the tangential to the wall velocity $v_\tau = v_i t_i$, where t_i are the tangent unit vector components in wall coordinates ($y^+ = \frac{v_\tau \Delta}{\nu}$, $v^+ = \frac{v_t}{v_\tau}$) results from the expressions $v^+ = \frac{1}{\kappa} ln y^+ + B$ if $y^+ \geq y_c^+$ or $v^+ = y^+$ if $y^+ < y_c^+$.

Note that y_c^+ is deduced from solving $y_c^+ = \frac{1}{\kappa} ln y_c^+ + B$, with $\kappa = 0.41$ and $B = 5.5$. With known v_τ, the boundary conditions for k and ε are

$$\begin{aligned} k_P &= \frac{v_\tau^2}{\sqrt{c_\mu}}, & \varepsilon_P &= \frac{v_\tau^3}{\kappa \Delta}, & &\text{if} \quad y^+ \geq y_c^+ \\ k_P &= \frac{v_\tau^2}{\sqrt{c_\mu}} \left(\frac{y^+}{y_c^+} \right)^2, & \varepsilon_P &= k_P^{\frac{3}{2}} \frac{1 + \frac{5.3\nu}{\sqrt{k_P}\Delta}}{\kappa c_\mu^{-\frac{3}{4}} \Delta}, & &\text{if} \quad y^+ < y_c^+ \end{aligned} \tag{17}$$

Similar to the definition of v_τ, eq. 16, the adjoint friction velocity u_τ at each S_W node is defined by

$$u_\tau^2 = (\nu + \nu_t) \left(\frac{\partial u_i}{\partial x_j} + \frac{\partial u_j}{\partial x_i} \right) n_j t_i \tag{18}$$

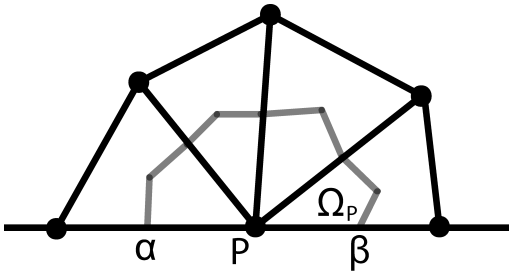

Figure 3: The adjoint technique with wall functions: A vertex-centered finite volume Ω_P associated with the solid "wall" (horizontal line) node P. Note that the real wall lies underneath the horizontal line sketched in this figure, at a distance Δ.

and is computed using the expression [12]

$$u_\tau^2 = \frac{1}{c_v}\left[2u_k t_k v_\tau - \left(\nu + \frac{\nu_t}{Pr_k}\right)\frac{\partial k_a}{\partial x_j}n_j\frac{\delta k}{\delta v_\tau} - \left(\nu + \frac{\nu_t}{Pr_\varepsilon}\right)\frac{\partial \varepsilon_a}{\partial x_j}n_j\frac{\delta \varepsilon}{\delta v_\tau}\right] \tag{19}$$

applied to the computation of the adjoint viscous fluxes at the "wall" nodes.

On the other hand, for the Spalart-Allmaras model (cell-centered finite-volume scheme, no-slip condition at the solid wall boundary faces) the wall function technique is based on a single formula modeling both the inner sublayer and the logarithmic region of the turbulent boundary layer

$$f_{WF} = y^+ - v^+ - e^{-\kappa B}\left[e^{\kappa v^+} - 1 - \kappa v^+ - \frac{(\kappa v^+)^2}{2} - \frac{(\kappa v^+)^3}{6}\right] = 0 \tag{20}$$

and similar expressions for the adjoint friction velocity may be derived, resulting to the condition of zero adjoint friction velocity. Indicative applications of the adjoint wall function technique are shown in figs. 4 and 5.

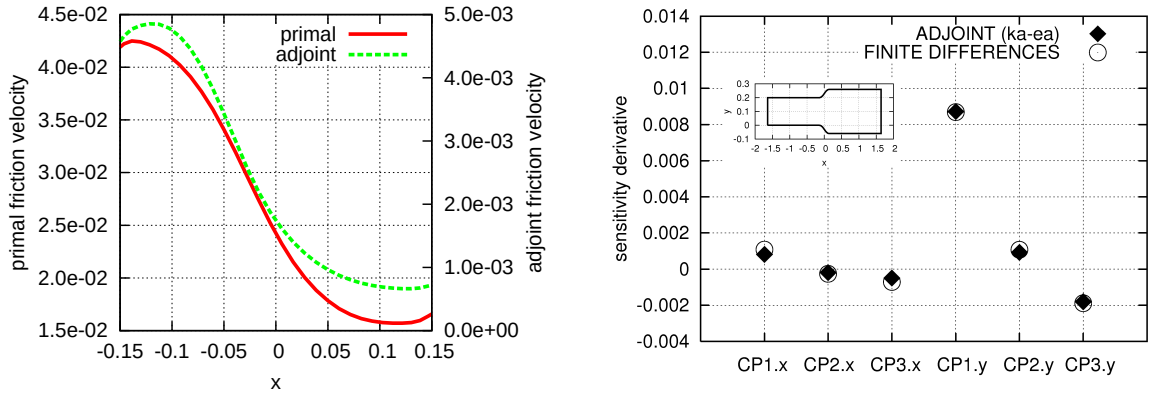

Figure 4: Adjoint to the high-Re Launder–Sharma $k-\epsilon$ model: Optimization of an axial diffuser using the adjoint wall function technique. Left: Friction velocity v_τ and squared adjoint friction velocity u_τ^2 distributions along its lower wall. Right: Sensitivity derivatives of F w.r.t. the design variables, i.e. the coordinates of Bézier control points parameterizing its side walls. The adjoint wall function method perfectly matches the sensitivity derivatives computed using finite differences (FD).

3 ROBUST DESIGN USING HIGH-ORDER SENSITIVITY ANALYSIS

In aerodynamics, robust design methods aim at optimizing a shape in a range of operating conditions, or by considering the effect of environmental uncertainties, such as manufacturing

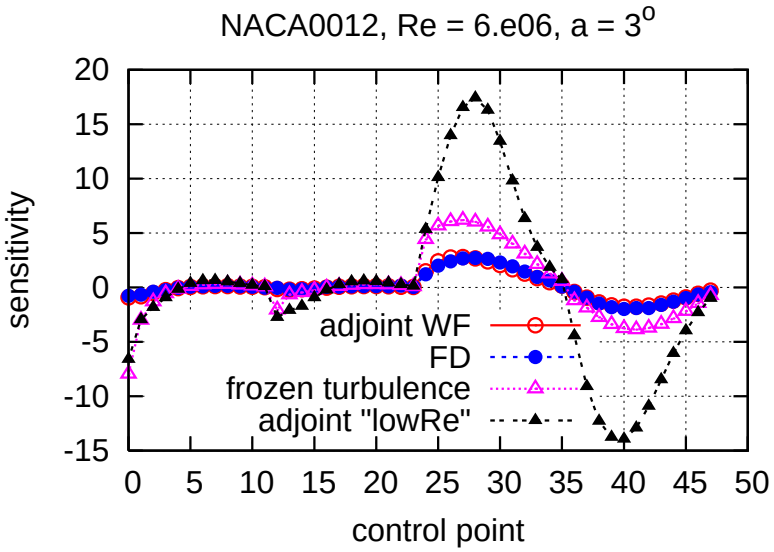

Figure 5: Adjoint to the high-Re Spalart–Allmaras model, NACA0012, $\alpha_\infty = 3^o$: Drag sensitivities computed using the proposed method (marked as "adjoint WF") are compared to the outcome of FD and the adjoint method using the "frozen turbulence" assumption and the adjoint method with the "low–Reynolds" approach (different scale on the vertical axis). The latter implies that the turbulence model is differentiated but the differentiation of the wall functions is disregarded. The first 24 points correspond to the derivatives w.r.t. the x coordinates of the suction and pressure side control points while the last 24 to those w.r.t. the y coordinates.

imprecisions, fluctuations of the flow conditions, etc. The latter depend on the so-called environmental variables $\mathbf{c}\,(c_i, i \in [1, M])$. In robust design problems, the function to be minimized can be expressed as $\widehat{F} = \widehat{F}\,(\mathbf{b}, \mathbf{c}, \mathbf{U}(\mathbf{b}, \mathbf{c}))$, to denote the dependency of $\widehat{F}$ on the flow variables $\mathbf{U}$, the design variables $\mathbf{b}\,(b_l, l \in [1, N])$ which parameterize the aerodynamic shape and the environmental variables $\mathbf{c}\,(c_i, i \in [1, M])$. Let us associate a probability density function $g(\mathbf{c})$ with $\mathbf{c}$. In the so-called Second-Order Second-Moment (SOSM) approach, the function $\widehat{F}$ to be minimized in a robust design problem combines the mean value μ_F and the variance ${\sigma_F}^2$ of F, namely

$$\mu_F(\mathbf{b}, \mathbf{c}) = \int F g(\mathbf{c}) d\mathbf{c} \simeq F + \frac{1}{2}\left[\frac{\delta^2 F}{\delta c_i^2}\right]_{\overline{\mathbf{c}}} \sigma_i^2 \tag{21}$$

$${\sigma_F}^2(\mathbf{b}, \mathbf{c}) = \int (F - \mu_F)^2 g(\mathbf{c}) d\mathbf{c} \simeq \left[\frac{\delta F}{\delta c_i}\right]^2_{\overline{\mathbf{c}}} \sigma_i^2 + \frac{1}{2}\left[\frac{\delta^2 F}{\delta c_i \delta c_j}\right]^2_{\overline{\mathbf{c}}} \sigma_i^2 \sigma_j^2 \tag{22}$$

where the gradients are evaluated at the mean values $\overline{\mathbf{c}}$ of the environmental variables.

Based on the previous definitions, in robust design, $\widehat{F}$ becomes

$$\widehat{F}(\mathbf{b}, \mathbf{c}) = w_1 \mu_F + w_2 \sigma_F^2 \tag{23}$$

where w_1 and w_2 are user-defined weights.

To compute $\widehat{F}$, efficient and accurate methods to compute first- and second-order derivatives of F w.r.t. the environmental variables are needed.

3.1 Computation of Statistical Moments using Second-Order Taylor Expansion

In aerodynamic optimization, the computation of the Hessian F subject to the constraint of satisfying the flow equations can be conducted in at least four different ways, as briefly exposed

below. All of them can be set up in either discrete or continuous form [14, 15, 16]. It is simpler, however, to present them in discrete form, where R_i and U_i stand for the discretized residual of the flow equations and the flow variables at node i, respectively. In discrete form, the first-order variation rate of F w.r.t. to $c_i, i=1,\ldots,N$ is given by

$$\frac{dF}{dc_i} = \frac{\partial F}{\partial c_i} + \frac{\partial F}{\partial U_k}\frac{dU_k}{dc_i} \tag{24}$$

whereas

$$\frac{dR_m}{dc_i} = \frac{\partial R_m}{\partial c_i} + \frac{\partial R_m}{\partial U_k}\frac{dU_k}{dc_i} = 0 \tag{25}$$

Solving eq. 25 for $\frac{dU_k}{dc_i}$, at the cost of N equivalent flow solutions (EFS; this is more or less the cost of solving the primal equations) and, then, computing $\frac{dF}{dc_i}$ from eq. 24 is straightforward but costly and will be referred to as the Direct Differentiation (DD) method. Since its cost scales with N, the Adjoint Variable (AV) method was proposed instead. The adjoint variables Ψ_i are computed by numerically solving the adjoint system of equations

$$R_k^\Psi = \frac{\partial F}{\partial U_k} + \Psi_m \frac{\partial R_m}{\partial U_k} = 0 \tag{26}$$

and computing

$$\frac{dF}{dc_i} = \frac{\partial F}{\partial c_i} + \Psi_m \frac{\partial R_m}{\partial c_i} \tag{27}$$

In discrete form, to compute the Hessian of F, the straightforward extension of the DD method for the gradient computation is the so-called DD-DD approach, in which $\frac{d^2F}{dc_i dc_j}$ can be computed by

$$\frac{d^2F}{dc_i dc_j} = \frac{\partial^2 F}{\partial c_i \partial c_j} + \frac{\partial^2 F}{\partial c_i \partial U_k}\frac{dU_k}{dc_j} + \frac{\partial^2 F}{\partial U_k \partial c_j}\frac{dU_k}{dc_i} + \frac{\partial^2 F}{\partial U_k \partial U_m}\frac{dU_k}{dc_i}\frac{dU_m}{dc_j} + \frac{\partial F}{\partial U_k}\frac{d^2U_k}{dc_i dc_j} \tag{28}$$

where the sensitivities $\frac{d^2U_k}{dc_i dc_j}$ are computed by solving ($\frac{dU_k}{dc_i}$ being already known from the solution of eqs. 25).

$$\frac{d^2R_n}{dc_i dc_j} = \frac{\partial^2 R_n}{\partial c_i \partial c_j} + \frac{\partial^2 R_n}{\partial c_i \partial U_k}\frac{dU_k}{dc_j} + \frac{\partial^2 R_n}{\partial U_k \partial c_j}\frac{dU_k}{dc_i} + \frac{\partial^2 R_n}{\partial U_k \partial U_m}\frac{dU_k}{dc_i}\frac{dU_m}{dc_j} + \frac{\partial R_n}{\partial U_k}\frac{d^2U_k}{dc_i dc_j} = 0 \tag{29}$$

The DD-DD approach cannot avoid also the computation of $\frac{dU_k}{dc_i}$ and, thus its computational cost is equal to $N + \frac{N(N+1)}{2}$ EFS in total (excluding the cost for solving the flow equations). So, the DD-DD approach scales with N^2 being too expensive for use in real–world optimization.

Two less expensive approaches to compute of the Hessian of F are the AV-DD (AV for the gradient and DD for the Hessian) and AV-AV ones. As shown in [16], both cost an many as $2N+1$ EFS. It can be shown that, in either discrete or continuous form, the fourth alternative way, i.e. the DD-AV approach (DD for the gradient and AV for the Hessian), is the most efficient one to compute the Hessian matrix. In DD-AV, the Hessian matrix is computed by

$$\begin{aligned}\frac{d^2F}{dc_i dc_j} = &\frac{\partial^2 F}{\partial c_i \partial c_j} + \Psi_n \frac{\partial^2 R_n}{\partial c_i \partial c_j} + \left(\frac{\partial^2 F}{\partial U_k \partial U_m} + \Psi_n \frac{\partial^2 R_n}{\partial U_k \partial U_m}\right)\frac{dU_k}{dc_i}\frac{dU_m}{dc_j} \\ &+ \left(\frac{\partial^2 F}{\partial c_i \partial U_k} + \Psi_n \frac{\partial^2 R_n}{\partial c_i \partial U_k}\right)\frac{dU_k}{dc_j} + \left(\frac{\partial^2 F}{\partial U_k \partial c_j} + \Psi_n \frac{\partial^2 R_n}{\partial U_k \partial c_j}\right)\frac{dU_k}{dc_i}\end{aligned} \tag{30}$$

where $\frac{dU_k}{dc_i}$ result from DD and Ψ_m is computed by solving the (same) adjoint equation, eq. 26. The total computational cost of DD-AV is equal to $N+1$ EFS.

3.2 Robust Shape Optimization using Third-Order Sensitivities

If the optimization problem of minimizing the combination of the two first statistical moments is to be solved using a stochastic method (such as an evolutionary algorithm), the methods presented above can be used to compute μ_F and ${\sigma_F}^2$. However, if a gradient-based method is selected to solve the problem, the gradient $\widehat{F}$ w.r.t. the design variables b_q must be available. By differentiating eq. 23 w.r.t. b_q, this becomes

$$\frac{\delta \widehat{F}}{\delta b_q} = w_1 \left(\frac{\delta F}{\delta b_q} + \frac{1}{2} \frac{\delta^3 F}{\delta c_i^2 \delta b_q} \sigma_i^2 \right) + w_2 \frac{2 \frac{\delta F}{\delta c_i} \frac{\delta^2 F}{\delta c_i \delta b_q} \sigma_i^2 + \frac{\delta^2 F}{\delta c_i \delta c_j} \frac{\delta^3 F}{\delta c_i \delta c_j \delta b_q} \sigma_i^2 \sigma_j^2}{2 \sqrt{\left[\frac{\delta F}{\delta c_i} \right]^2 \sigma_i^2 + \frac{1}{2} \left[\frac{\delta^2 F}{\delta c_i \delta c_j} \right]^2 \sigma_i^2 \sigma_j^2}} \tag{31}$$

From eq. 31, $\frac{\delta \widehat{F}}{\delta b_q}$ requires the computation of up to third-order mixed sensitivities w.r.t. c_i and b_q, such as $\frac{\delta^3 F}{\delta c_i \delta c_j \delta b_q}$. The computation of the second and third-order sensitivity derivatives is presented in detail in [17, 18]. For instance, $\frac{d^2 F}{dc_i dc_j db_q}$ is computed using the expression

$$\begin{aligned}
\frac{d^3 F}{dc_i dc_j db_l} &= \frac{\partial^3 F}{\partial c_i \partial c_j \partial b_l} + \frac{\partial^3 F}{\partial c_i \partial b_l \partial U_{k,d}} \cdot \frac{dU_{k,d}}{dc_j} + \frac{\partial^3 F}{\partial c_j \partial b_l \partial U_{k,d}} \cdot \frac{dU_{k,d}}{dc_i} \\
&+ \frac{\partial^3 F}{\partial b_l \partial U_{k,d} \partial U_{m,e}} \cdot \frac{dU_{k,d}}{dc_i} \cdot \frac{dU_{m,e}}{dc_j} + \frac{\partial^2 F}{\partial b_l \partial U_{k,d}} \cdot \frac{d^2 U_{k,d}}{dc_i dc_j} \\
&+ \mathcal{K}_{n,a}^{i,j} \frac{\partial R_{n,a}}{\partial b_l} + \mathcal{L}_{n,a}^{j} \left(\frac{\partial^2 R_{n,a}}{\partial c_i \partial b_l} + \frac{\partial^2 R_{n,a}}{\partial b_l \partial U_{k,d}} \cdot \frac{dU_{k,d}}{dc_i} \right) \\
&+ \mathcal{M}_{n,a}^{i} \left(\frac{\partial^2 R_{n,a}}{\partial c_j \partial b_l} + \frac{\partial^2 R_{n,a}}{\partial b_l \partial U_{k,d}} \cdot \frac{dU_{k,d}}{dc_j} \right) \\
&+ \mathcal{N}_{n,a} \left(\frac{\partial^3 R_{n,a}}{\partial c_i \partial c_j \partial b_l} + \frac{\partial^3 R_{n,a}}{\partial c_i \partial b_l \partial U_{k,d}} \cdot \frac{dU_{k,d}}{dc_j} + \frac{\partial^3 R_{n,a}}{\partial c_j \partial b_l \partial U_{k,d}} \cdot \frac{dU_{k,d}}{dc_i} \right. \\
&+ \left. \frac{\partial^3 R_{n,a}}{\partial b_l \partial U_{k,d} \partial U_{m,e}} \cdot \frac{dU_{k,d}}{dc_i} \cdot \frac{dU_{m,e}}{dc_j} + \frac{\partial^2 R_{n,a}}{\partial b_l \partial U_{k,d}} \cdot \frac{d^2 U_{k,d}}{dc_i dc_j} \right)
\end{aligned} \tag{32}$$

where the additional adjoint variables $\mathcal{N}_{n,a}$ should satisfy the equation

$$\frac{\partial F}{\partial U_{k,d}} + \mathcal{N}_{n,a} \frac{\partial R_{n,a}}{\partial U_{k,d}} = 0 \tag{33}$$

the variables $\mathcal{L}_{n,a}^{j}$ are computed by solving

$$\frac{\partial^2 F}{\partial c_j \partial U_{k,d}} + \frac{\partial^2 F}{\partial U_{k,d} \partial U_{m,e}} \cdot \frac{dU_{m,e}}{dc_j} + \mathcal{L}_{n,a}^{j} \frac{\partial R_{n,a}}{\partial U_{k,d}} + \mathcal{N}_{n,a} \left(\frac{\partial^2 R_{n,a}}{\partial c_j \partial U_{k,d}} + \frac{\partial^2 R_{n,a}}{\partial U_{k,d} \partial U_{m,e}} \cdot \frac{dU_{m,e}}{dc_j} \right) = 0 \tag{34}$$

and $\mathcal{M}^i_{n,a}$ are computed from the equation

$$\begin{aligned}
&\frac{\partial^3 F}{\partial c_i \partial c_j \partial U_{q,g}} + \frac{\partial^3 F}{\partial c_i \partial U_{k,d} \partial U_{q,g}} \cdot \frac{dU_{k,d}}{dc_j} + \frac{\partial^3 F}{\partial c_j \partial U_{k,d} \partial U_{q,g}} \cdot \frac{dU_{k,d}}{dc_i} \\
+ &\frac{\partial^3 F}{\partial U_{k,d} \partial U_{m,e} \partial U_{q,g}} \cdot \frac{dU_{k,d}}{dc_i} \cdot \frac{dU_{m,e}}{dc_j} + \frac{\partial^2 F}{\partial U_{k,d} \partial U_{q,g}} \cdot \frac{d^2 U_{k,d}}{dc_i dc_j} + \mathcal{K}^{i,j}_{n,a} \frac{\partial R_{n,a}}{\partial U_{q,g}} \\
+ &\mathcal{L}^j_{n,a} \left(\frac{\partial^2 R_{n,a}}{\partial c_i \partial U_{q,g}} + \frac{\partial^2 R_{n,a}}{\partial U_{k,d} \partial U_{q,g}} \cdot \frac{dU_{k,d}}{dc_i} \right) + \mathcal{M}^i_{n,a} \left(\frac{\partial^2 R_{n,a}}{\partial c_j \partial U_{q,g}} + \frac{\partial^2 R_{n,a}}{\partial U_{k,d} \partial U_{q,g}} \cdot \frac{dU_{k,d}}{dc_j} \right) \\
+ &\mathcal{N}_{n,a} \left(\frac{\partial^3 R_{n,a}}{\partial c_i \partial c_j \partial U_{q,g}} + \frac{\partial^3 R_{n,a}}{\partial c_i \partial U_{k,d} \partial U_{q,g}} \cdot \frac{dU_{k,d}}{dc_j} + \frac{\partial^3 R_{n,a}}{\partial c_j \partial U_{k,d} \partial U_{q,g}} \cdot \frac{dU_{k,d}}{dc_i} \right. \\
+ &\left. \frac{\partial^3 R_{n,a}}{\partial U_{k,d} \partial U_{m,e} \partial U_{q,g}} \cdot \frac{dU_{k,d}}{dc_i} \cdot \frac{dU_{m,e}}{dc_j} + \frac{\partial^2 R_{n,a}}{\partial U_{k,d} \partial U_{q,g}} \cdot \frac{d^2 U_{k,d}}{dc_i dc_j} \right) = 0
\end{aligned} \tag{35}$$

An application of the robust design algorithm is illustrated in fig. 6 in the optimization of a 2D symmetric cascade, [18]. The design variable consist of the shape controlling parameters and the uncertain parameters consist of the flow conditions.

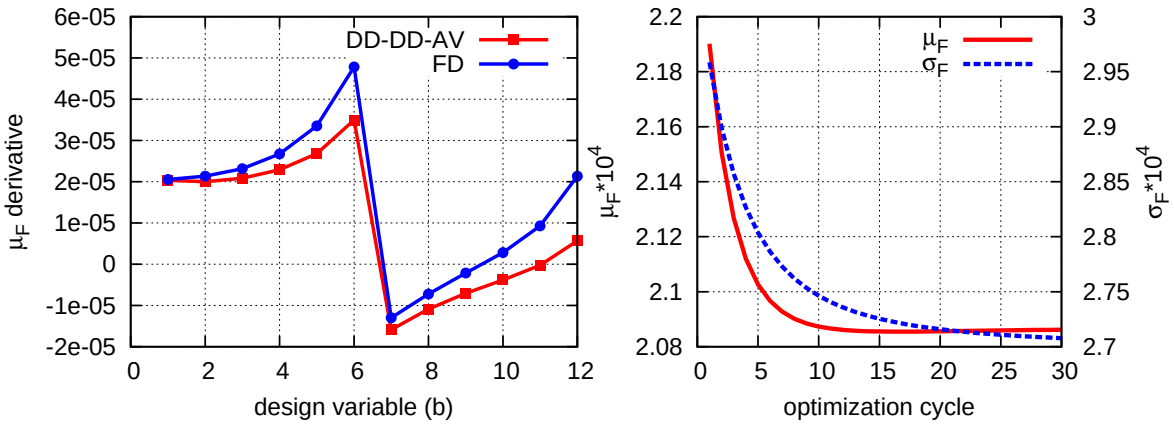

Figure 6: Robust inverse design of a 2D symmetric cascade. Left: Comparison of sensitivities $\frac{\delta \mu_F}{\delta b_q}$ (b_q are the coordinates of Bézier control points) computed using the proposed method and finite differences (FD). the proposed method practically matches the third derivatives captured by FD. Right: convergence of the mean value and standard deviation of F using $w_1 = 0.7, w_2 = 0.3$. From [18].

4 OTHER TOPICS RELATED TO ADJOINT APPROACHES AND OPTIMIZATION

The last section summarizes some other recent achievements regarding continuous adjoint methods.

Low-cost truncated Newton methods: To avoid the computation of Hessian (in large scale optimization problems, in particular), the truncated Newton algorithm can be used instead, [19]. The adjoint approach followed by the direct differentiation of both the flow and adjoint equations (AV-DD) is proved to be the most efficient way to compute the product of the Hessian matrix with any vector required by the truncated Newton algorithm, in which the Newton equations are solved via the conjugate gradient method. Considering that the cost of solving either the adjoint or the direct differentiation equations is approximately equal to that of solving the

flow equations, the cost per Newton iteration scales linearly with the number of conjugate gradient steps required, rather than the (much higher, in large scale problems) number of design variables (if the Hessian itself was computed). The efficiency of the truncated Newton method is demonstrated in fig. 7.

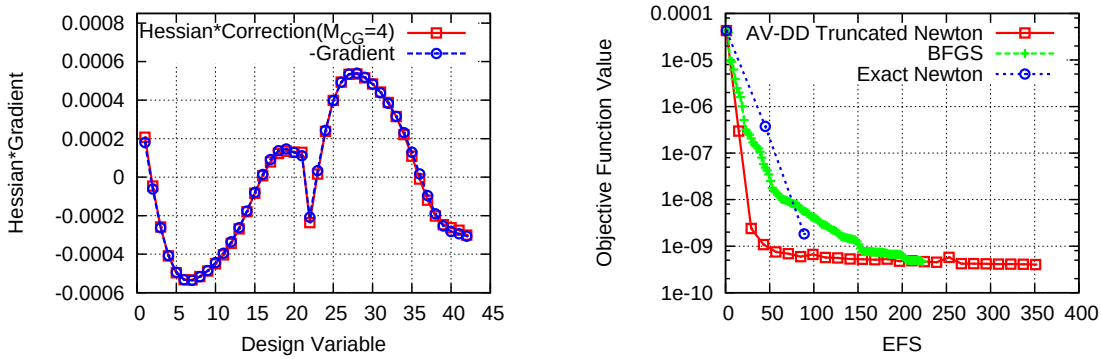

Figure 7: Design of a 2D airfoil cascade (42 degrees of freedom) using the truncated Newton method: Left: Validation of the solution of the Newton equation with $M_{CG} = 4$ conjugate gradient steps; the product of the exact Hessian matrix and the computed correction is compared to the exact gradient value. Right: Comparison of the convergence rates of the AV-DD truncated Newton method (with $M_{CG} = 4$) with other second-order methods (BFGS and exact Newton). From [19].

Adjoint methods for active flow control with blowing/suction jets: The continuous adjoint method has been used as a low-cost tool to derive information regarding the optimal location and type of steady suction/ blowing jets, used to control flow separation. The derivatives of this objective function with respect to hypothetical normal jet velocities along the walls are computed using the continuous adjoint method.

Slot	*Amplitude*
1	0.0160
2	0.0301
3	0.0315
4	0.0068
5	−0.0400
6	−0.0596
7	−0.0147
8	0.0776

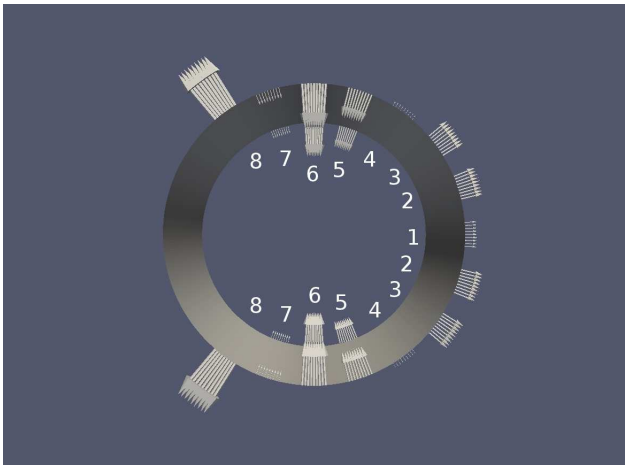

Figure 8: Time-averaged drag minimization of the flow around a cylinder: Optimal amplitude of each pulsating jet after seven optimization cycles.

Adjoint methods for topology optimization: Continuous adjoint methods for solving topology optimization problems for laminar and turbulent ducted flows of incompressible fluids, with or without heat transfer, have been developed, [20]. For turbulent flows, the adjoint approach is

exact, i.e. includes the differentiation of the turbulence model. In manifold flows, constraints on the percentage of the incoming flow rate directed to each exit boundary can be imposed.

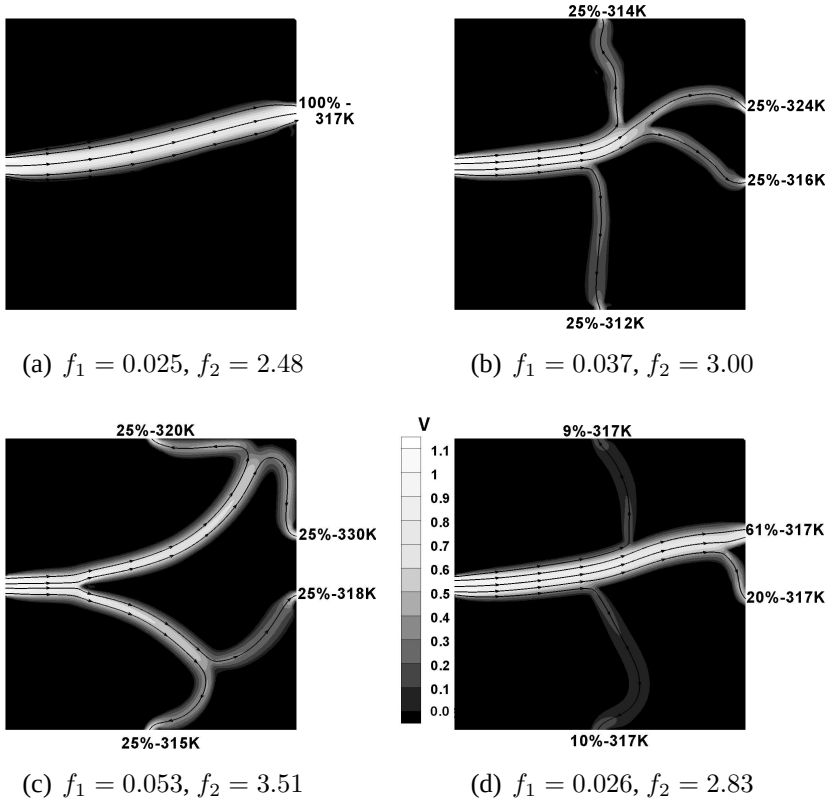

(a) $f_1 = 0.025$, $f_2 = 2.48$ (b) $f_1 = 0.037$, $f_2 = 3.00$

(c) $f_1 = 0.053$, $f_2 = 3.51$ (d) $f_1 = 0.026$, $f_2 = 2.83$

Figure 9: Unconstrained topology optimization of the one inlet/four outlet duct aiming at minimum $F = f_1$ (top left). Constrained topology optimization enforcing 25% of the incoming flow rate to exit from each outlet for, minimum $F = f_1$ (top right) and minimum $F = f_1 - 0.01 f_2$ (bottom left). Constrained topology optimization subject to the constraint of equal mean temperature at each outlet for minimum $F = f_1 - 0.01 f_2$ (bottom right). Velocity iso-areas and flow trajectories in the optimal solutions for the four cases. From [20].

4.1 INDUSTRIAL APPLICATIONS

In fig. 10, the application of the presented adjoint approaches to three industrial problems is presented. The first case deals with the blade optimization of a $3D$ peripheral compressor cascade in which the objective is the minimization of entropy losses within the flow passage, [21]. The second one is concerned with the shape optimization of a Francis turbine runner in order to achieve the desired target head and the last with the shape optimization of the Volkswagen L1 concept car, targeting minimum drag force, [22].

Acknowledgments

Parts of the relevant research ware funded by Volkswagen AG (Group Research, K-EFFG/V, Wolfsburg, Germany) and Icon Technology and Process Consulting Ltd. Research related to topology optimization and the computation of second–order derivatives was partially supported by Basic Research projects funded by the National Technical University of Athens.

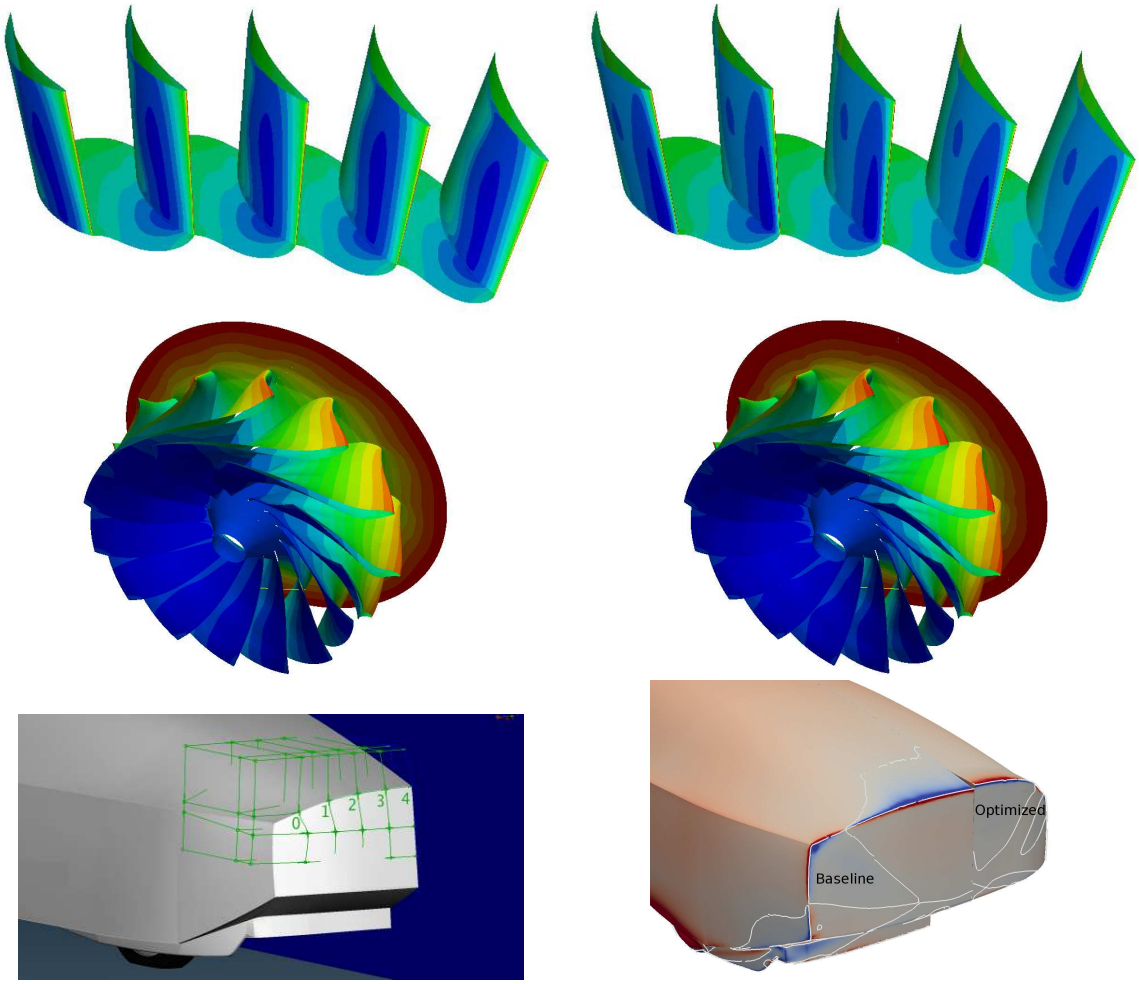

Figure 10: Top: Shape optimization of a 3D peripheral compressor cascade, targeting minimum entropy generation rate within the flow passage with constraints on the blade thickness. Pressure distributions over the initial (left) and optimal (right) blade geometries; from [21]. Mid: Optimization of a Francis runner blade for increased hydraulic head (by $1.5m$) subject to a number of flow constraints. Pressure distributions over the initial (left) and optimal (right) runners. Bottom: Optimization of the VW L1 concept car targeting minimum drag force. Parameterization of the rear part of the geometry by drawing morphing boxes (left) and comparative view of the baseline and optimized geometries with the corresponding sensitivity derivatives; from [22].

REFERENCES

[1] P. Spalart and S. Allmaras: A one-equation turbulence model for aerodynamic flows. *AIAA Paper*, 04(39), 1992.

[2] W. Jones, B. Launder: The prediction of laminarization with a two–equation model of turbulence. *International Journal of Heat And Mass Transfer*, 15 (1972), 301–314.

[3] B.J. Lee, C. Kim: Automated design methodology of turbulent internal flow using discrete adjoint formulation. *Aerospace Science and Technology*, 11 (2007), 163-173.

[4] D.J. Mavriplis: Discrete adjoint–based approach for optimization problems on three–dimensional unstructured meshes. *AIAA Journal*, 45 (2007), 740-750.

[5] O. Pironneau: On optimum design in fluid mechanics. *Journal of Fluid Mechanics*, 64 (1974), 97-110.

[6] A. Jameson: Aerodynamic design via control theory. *Journal of Scientific Computing*, 3 (1988), 233-260.

[7] W.K. Anderson, V. Venkatakrishnan: Aerodynamic design optimization on unstructured grids with a continuous adjoint formulation. *AIAA Paper*, 97-0643, 1997.

[8] D.I. Papadimitriou, K.C. Giannakoglou: A continuous adjoint method with objective function derivatives based on boundary integrals for inviscid and viscous flows. *Journal of Computers and Fluids*, 36 (2007), 325-341.

[9] C. Othmer: A continuous adjoint formulation for the computation of topological and surface sensitivities of ducted flows. *International Journal for Numerical Methods in Fluids*, 58 (2008), 861-877.

[10] A.S. Zymaris, D.I. Papadimitriou, K.C. Giannakoglou, C. Othmer: Continuous adjoint approach to the Spalart-Allmaras turbulence model for incompressible flows, *Computers & Fluids*, 38 (2009), 1528–1538.

[11] A. Bueno-Orovio, C. Castro, F. Palacios, E. Zuazua: Continuous Adjoint Approach for the SpalartAllmaras Model in Aerodynamic Optimization *AIAA Journal*, 50 (2012), 631–646.

[12] A.S. Zymaris, D.I. Papadimitriou, K.C. Giannakoglou, C. Othmer: Adjoint wall functions: A new concept for use in aerodynamic shape optimization, *Journal of Computational Physics*, 229 (2010), 5228–5245.

[13] E.M. Papoutsis-Kiachagias, A.S. Zymaris, I.S. Kavvadias, D.I. Papadimitriou, KC. Giannakoglou: The continuous adjoint approach to the k-ϵ turbulence model for shape optimization and optimal active control of turbulent flows. *Engineering Optimization*, (to appear) 2014.

[14] D.I. Papadimitriou, K.C. Giannakoglou: Computation of the Hessian matrix in aerodynamic inverse design using continuous adjoint formulations. *Computers & Fluids*, 37 (2008), 1029–1039.

[15] D.I. Papadimitriou, K.C. Giannakoglou: The continuous direct-adjoint approach for second-order sensitivities in viscous aerodynamic inverse design problems, *Computers & Fluids*, 38 (2008), 1539–1548.

[16] D.I. Papadimitriou, K.C. Giannakoglou: Aerodynamic shape optimization using adjoint and direct approaches, *Archives of Computational Methods in Engineering*, 15 (2008), 447–488.

[17] E.M. Papoutsis-Kiachagias, D.I. Papadimitriou, K.C. Giannakoglou: Robust design in aerodynamics using third-order sensitivity analysis based on discrete adjoint. Application to quasi-1D flows. *International Journal for Numerical Methods in Fluids*, 69 (2012), 691-709.

[18] E.M. Papoutsis-Kiachagias, D.I. Papadimitriou, K.C. Giannakoglou: On the optimal use of adjoint methods in aerodynamic robust design problems. *CFD and OPTIMIZATION 2011, ECCOMAS Thematic Conference*, Antalya, Turkey, 2011.

[19] D.I. Papadimitriou, K.C. Giannakoglou: Aerodynamic Design using the Truncated Newton Algorithm and the Continuous Adjoint Approach. *International Journal for Numerical Methods in Fluids*, 68 (2012), 724-739.

[20] E.M. Papoutsis-Kiachagias, E.A. Kontoleontos, A.S. Zymaris, D.I. Papadimitriou, K.C. Giannakoglou: Constrained topology optimization for laminar and turbulent flows, including heat transfer. *EUROGEN Conference 2011*, Capua, Italy.

[21] D.I. Papadimitriou, K.C. Giannakoglou: Compressor blade optimization using a continuous adjoint formulation. *ASME TURBO EXPO*, GT2006/90466, 8-11 May 2006, Barcelona, Spain.

[22] C. Othmer, E. Papoutsis-Kiachagias, K. Haliskos: CFD Optimization via Sensitivity-Based Shape Morphing. *4th ANSA & μETA International Conference*, Thessaloniki, Greece, 2011.